J. Fluid Mech. (2008), *vol.* 603, *pp.* 245–270.
doi:10.1017/S0022112008001134 Printed in the United Kingdom

Analytic study of developing flows in a tube laden with non-evaporating and evaporating drops via a modified linearization of the two-phase momentum equations

S. KHOSID[1]† AND Y. TAMBOUR[2]‡

[1]Department of Applied Mathematics, Technion–Israel Institute of Technology, Haifa 32000, Israel
[2]Department of Aerospace Engineering, Technion–Israel Institute of Technology, Haifa 32000, Israel

(Received 30 May 2007 and in revised form 13 February 2008)

A novel modification of the classical Langhaar linearization of the mutually coupled momentum equations for developing two-phase flows in circular ducts is presented. This modification enables us to treat: (i) flows developing from spatially periodic initial velocity distributions without the presence of droplets, and (ii) two-phase flows in which monosize, non-evaporating and evaporating droplets suspended in a developing gas flow of an initially uniform velocity distribution exchange momentum with the host-gas flow. New solutions are presented for the downstream evolution in the velocity profiles which develop from spatially periodic initial velocity distributions that eventually reach the fully developed Poiseuille velocity profile. These solutions are validated by employing known numerical procedures, providing strong support for the physical underpinnings of the present modified linearization. New solutions are also presented for the evolution in drop velocities and vapour spatial distributions for evaporating droplets suspended in an initially uniform velocity profile of the host gas. Asymptotic solutions are presented for the flow region which lies very close to the inlet of the tube, where the relative velocity between the droplets and the host gas is high, and thus the velocity fields of the two phases are mutually coupled. These solutions provide new explicit formulae for the droplet velocity field as a function of the initial conditions and droplet diameter (relative to the tube diameter) for non-evaporating drops, and also as a function of evaporation rate for evaporating drops.

1. Introduction

In many applications of practical interest, evaporating drops are being transported by gas flows and thus the two-phase flow fields become mutually coupled. Hence, the study of evaporating drops suspended in various flow fields has been of continued interest in fluid mechanics research, e.g. Katoshevski & Tambour (1993, 1995), Miller & Bellan (1999), Leboissetier, Okong'o & Bellan (2005), Le Clercq & Bellan (2005). In research on the combustion of liquid fuel droplets and sprays, it is important to analyse the dynamics of the evaporating drops and the spread of fuel vapours by the gaseous flow field, e.g. Borghi (1996), Candel *et al.* (1999), Laurent & Massot (2001), Laurent *et al.* (2004), Meng *et al.* (2005), Réveillon & Vervisch (2005), Nakamura

†Present address: RAFAEL, Armament Development Authority, Israel.
‡Author to whom correspondence should be addressed: ytambour@aerodyne.technion.ac.il.

et al. (2005), Laurent (2006). The above problems are usually addressed by employing numerical solutions. Parallel to these efforts, analytical solutions have also been sought (Silverman, Greenberg & Tambour 1991; Tambour & Katoshevski 1994; Tambour 1995). These asymptotic (Silverman *et al.* 1991; Tambour & Katoshevski 1995) and other analytical solutions (Tambour & Katoshevski 1994; Anidjar, Greenberg & Tambour 1996) provide a relatively comfortable tool for gaining physical insight when analysing evaporating droplets suspended in gaseous flow fields and spray flames, and have the advantage of serving as a reference for the validation of numerical solutions (e.g. Khosid & Tambour 1993). Comprehensive asymptotic studies were also conducted by Schonberg & Hinch (1989) and Asmolov (1999) for analysing the lift forces acting on particles suspended in two-dimensional fully developed channel flows between two parallel plates.

The investigation of flows in ducts is important in its own right since it serves a large variety of traditional engineering disciplines such as biomechanics, aerospace and chemical engineering, in which circular and non-circular ducts are employed for instrumentation, heating and cooling devices, and the transportation of liquids and gases with and without droplets and solid particles. For example, the migration of solid particles in Poiseuille flows has been of continued interest since the Segré & Silberberg (1962) classical discovery that single rigid neutrally buoyant spheres migrate to an equilibrium position located at pipe radius $r = 0.6$. Recently, Matas *et al.* (2004*a*) and Matas, Morris & Guazzelli (2004*b*) extended this classical study to include the effects of the flow Reynolds number. The study of suspended evaporating sprays in developing flows in ducts is also of importance when analysing miniature combustion chambers, e.g. Chigier & Gemci (2002). In this regard, it is important to define the operating conditions under which the droplets fully vaporize at short distances in a developing flow in a tube, providing vapours for the miniature combustion chamber. In addition, the theoretical analysis of the behaviour of laminar spatially periodic gaseous flow fields may also provide insight into flames in turbulent flow fields. The reasoning behind the above observation lies in the well-known structure of turbulent flows which is characterized by a wide range of spatial–temporal scales and their associated motion which can be visualized as a cascade of eddies.

Based on the above-described behaviour of turbulent flow fields, Sivashinsky (1988) and later Berestycki & Sivashinsky (1991) successfully applied the cascade concept to large-scale turbulent premixed flames by modelling the flow field as a one-scale unidirectional spatially periodic flow field. Adopting Sivashinsky's approach, further understanding of the structure and response of premixed flames in a spatially periodic time-independent flow field was gained in a more recent study by Yu, Sung & Law (1994).

In combustion systems utilizing liquid fuels, the liquid is generally in the form of a spray. Greenberg & Cohen (1992) showed that spatially non-uniform distributions of droplet concentration and velocity can lead to asymmetrically distorted spray diffusion flames.

All the above-mentioned studies indicate the paramount importance of studying spatially periodic flows and the behaviour of evaporating sprays suspended in gaseous flow fields. Undertaking the latter study is the main goal of present paper. In the first part we will focus on laminar unidirectional spatially periodic time-independent developing gaseous flows in a circular duct. Then, flows developing from initially uniform velocities laden with non-evaporating and evaporating droplets will be analysed.

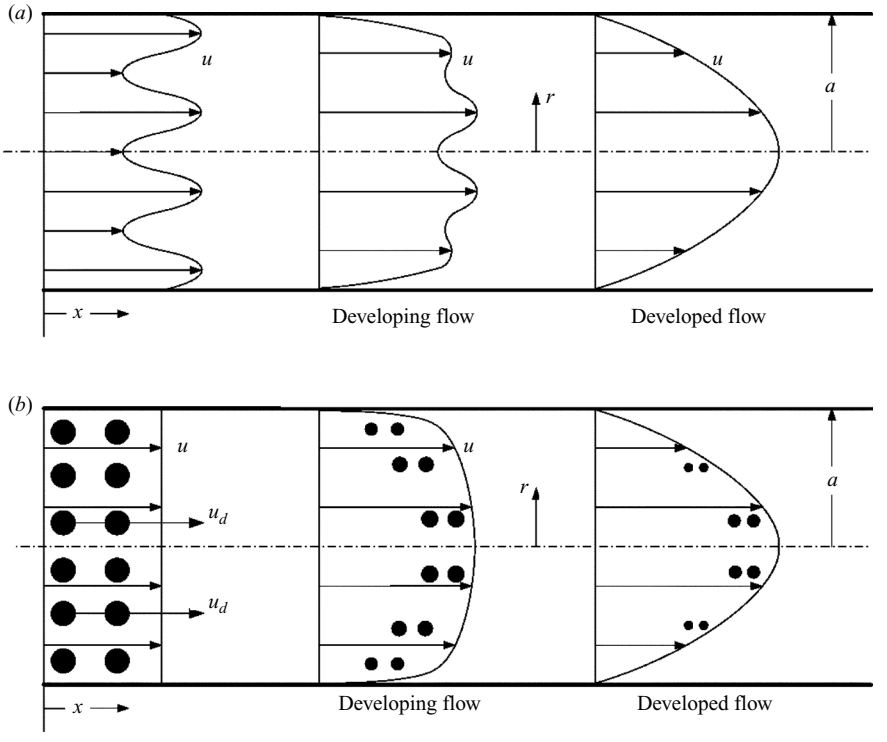

FIGURE 1. Schematic description of developing laminar flow in a circular duct: (*a*) gaseous flow of an initially spatially periodic velocity profile, (*b*) uniform initial velocity profile with initially monosize evaporating droplets. Note that the droplets are introduced into the tube at a velocity higher (or lower) than the host gas velocity.

A comprehensive review of the analytical work associated with flows in ducts was presented by Shah & London (1978). This excellent review covers almost 530 papers and represents the state of the art in 1978. Since then, dozens of papers have been published in that area. A literature survey that we carried out indicates that Langhaar's linearization is a very useful tool for treating developing flows in ducts since it allows one to solve the axial flow momentum equation analytically. It leads to satisfactory results when solving for the velocity profiles that develop from an initially uniform velocity distribution at the duct entrance. However, Langhaar's linearization is limited to treating initially uniform velocity distributions only, and to flow systems which do not contain droplets suspended in the flow field, whereas here we will treat spatially periodic initial velocity profiles and initially uniform flows laden with nonevaporating and evaporating drops.

The flow system under consideration is presented in figure 1. Detailed formulations of the governing equations for a developing flow in a duct and the explanation of Langhaar's linearization can be found in the literature, e.g. see Langhaar (1942), Shah & London (1978) and Ward-Smith (1980). Note that in order to linearize the momentum equation and solve it analytically, Langhaar (1942) introduced function γ, which is a function of axial position only. Then, the function γ was determined from the momentum equation evaluated at the centreline and from a momentum integral equation. The pressure drop was calculated separately from a mechanical energy integral equation.

Since our purpose is to treat (*a*) flows developing from initially spatially periodic velocity profiles, and (*b*) a developing initially uniform gaseous duct flow that exchanges momentum with droplets suspended in the flow field, we propose modifying Langhaar's linearization. Our modification will include a new function f and a velocity u_{bound} whereby a non-uniform initial velocity profile may be treated. The function f will be determined by using a mechanical-energy equation. The velocity u_{bound} is the velocity of the flow along the boundary between the decelerated and the accelerated zones of the developing flow. This modified linearization will also be employed here to analyse the behaviour of non-evaporating and evaporating monosize sprays which are suspended in an initially uniform developing duct flow. The mathematical treatment is presented below.

2. Flow developing from a non-uniform initial velocity profile in a circular duct

The governing equations for a steady-state incompressible developing flow in a duct (see figure 1) may be written (in a non-dimensional form) as
momentum

$$\frac{\mathrm{Du}}{\mathrm{Dt}} = u\frac{\partial u}{\partial x} + v\frac{\partial u}{\partial r} = -\frac{\mathrm{d}p}{\mathrm{d}x} + \frac{1}{r}\frac{\partial}{\partial r}\left(r\frac{\partial u}{\partial r}\right), \tag{2.1}$$

continuity

$$\frac{\partial u}{\partial x} + \frac{1}{r}\frac{\partial (rv)}{\partial r} = 0, \tag{2.2}$$

where the non-dimensional variables are defined as

$$u = \frac{u^*}{\bar{u}}, \quad v = \frac{v^* a}{\nu}, \quad x = \frac{x^* \nu}{\bar{u} a^2}, \quad r = \frac{r^*}{a} \quad p = \frac{p^*}{\rho \bar{u}^2}, \quad t = \frac{t^* a^2}{\nu}.$$

Here u^* and v^* are the axial and radial velocity components of the fluid, $\bar{u}$ is the mean value of u^*, x^* and r^* are the axial and radial coordinates, p^* is the pressure of the fluid, a is the radius of the duct, ρ is the fluid density, ν is the kinematic viscosity of the fluid, and t^* is the time.

In order to solve the momentum equation analytically, Langhaar (1942) suggested the following linearization:

$$\frac{\mathrm{D}u}{\mathrm{D}t} = -\frac{\mathrm{d}p}{\mathrm{d}x} + \frac{1}{r}\frac{\partial}{\partial r}\left(r\frac{\partial u}{\partial r}\right) = \gamma^2 u \tag{2.3}$$

whose solution

$$u = BI_0(\gamma r) + C \tag{2.4}$$

leads to satisfactory results when solving for velocity profiles that develop from an initially uniform velocity distribution at the duct entrance. In the above, I_0 is the zeroth-order Bessel function, γ is a function of x, and C is a constant.

The above solution must satisfy the no-slip and the non-permeability boundary conditions

$$u_{r=1} = v_{r=1} = 0 \tag{2.5}$$

and also the continuity integral equation

$$\int_0^1 ru\,\mathrm{d}r = \frac{1}{2}. \tag{2.6}$$

Employing (2.5) and (2.6), equation (2.4) yields the classical Langhaar's velocity profile

$$u_L = \frac{I_0(\gamma) - I_0(\gamma r)}{I_2(\gamma)} \tag{2.7}$$

which develops from a uniform profile $u = 1$, obtained by substituting $\gamma = \infty$ (which corresponds to the initial station $x = 0$) into (2.7), to the fully developed profile $u = 2(1-r^2)$, for $\gamma = 0$. Note, however, that there is no γ for which u_L can represent a non-uniform initial velocity profile, e.g. a spatially periodic profile. Thus, Langhaar's linearization is limited to treating only initially uniform velocity distributions, and as will be demonstrated later, even for an initially uniform velocity profile, if a liquid spray is suspended in the flow, one cannot obtain analytic solutions for the velocity field of the droplets that exchange momentum with the host-gas flow with the aid of Langhaar's linearization (and therefore one must resort to some other kind of linearization). Thus, it is the purpose of the present study to present a new form of linearization, which is a modification of Langhaar's linearization, in order to overcome the above-described shortcomings.

For flows which start from a non-uniform initial velocity profile (or in two-phase flows in which liquid droplets exchange momentum with the host-gas flow) we propose here a modification to (2.3) of the form

$$\frac{\mathrm{D}u}{\mathrm{D}t} = -\frac{\mathrm{d}p}{\mathrm{d}x} + \frac{1}{r}\frac{\partial}{\partial r}\left(r\frac{\partial u}{\partial r}\right) = \gamma^2(u - u_{bound}) \tag{2.8}$$

where u_{bound} is a function of γ and r and its functional form will be determined later.

A solution for (2.8) must satisfy the no-slip and the non-permeability boundary conditions (2.5) and also the continuity integral equation (2.6).

Now, let the initial velocity profile be non-uniform (but symmetrical in r), that is

$$u(x = 0, r) = 1 + \xi(r) \tag{2.9}$$

where

$$\int_0^1 r\xi(r)\,\mathrm{d}r = 0 \tag{2.10}$$

and

$$\xi(-r) = \xi(r). \tag{2.11}$$

We propose a new solution for the developing profile u of the form

$$u = [1 + f\xi(1)]u_L + f[\xi(r) - \xi(1)] \tag{2.12}$$

to be a solution of (2.8).

In the above u_L is the Langhaar profile (2.7) and $f(x)$ (or $f(\gamma)$) is an unknown function of x (or γ) to be sought. Since at $x = 0$ (where $u_L = 1$) equation (2.12) must reduce to the form of (2.9), the initial condition for f is

$$f(x = 0, \text{ i.e. } \gamma \to \infty) = 1. \tag{2.13}$$

At the other edge for $x \to \infty$ our solution must approach the fully developed profile which is represented here by u_L and hence the function f must satisfy

$$f(x \to \infty, \text{ i.e. } \gamma \to 0) = 0. \tag{2.14}$$

Next, since we require the pressure to be a function of x only, u_{bound} may be expressed as

$$u_{bound}(\gamma, r) = u(\gamma, r_{bound}) + f(\gamma)[\varphi(\gamma, r) - \varphi(\gamma, r_{bound})] \tag{2.15}$$

where

$$\varphi(\gamma, r) = \xi(r) - \frac{1}{\gamma^2}\frac{1}{r}\frac{\partial}{\partial r}\left(r\frac{\partial \xi(r)}{\partial r}\right) \tag{2.16}$$

and the radial position $r_{bound}(\gamma)$ is found from the condition

$$\frac{\partial u}{\partial \gamma}|_{r_{bound}} = 0. \tag{2.17}$$

Note that as the flow approaches its fully developed profile (i.e. as $\gamma \to 0$, then $u \to u_L$, and thus employing (2.7)), one obtains

$$\lim_{\gamma \to 0} r_{bound} = \frac{1}{\sqrt{3}} \approx 0.58. \tag{2.18}$$

In the above, r_{bound} is a boundary between the accelerated and the decelerated zones of the flow, and its final value 0.58 (see equation (2.18)) is very close to the value $r = 0.6$ where neutrally buoyant particles concentrate after the entrance region of a tube, as was first documented by Segré & Silberberg (1962) in their classical experiment. This analysis also agrees with Soo's assertion (Soo 1990) that the 'maximum concentration (of particles) occurs where the velocity gradient is least'.

The unknown function f will be evaluated below, but first we have to determine the axial pressure drop.

3. Determination of the axial pressure drop

To obtain the variation of the unknown function γ with the axial distance x:$\mathrm{d}x/\mathrm{d}\gamma$, Langhaar eliminated the pressure drop $\mathrm{d}p/\mathrm{d}x$ by comparing two equations. The first was the momentum equation (2.1) which was applied to the axis of symmetry (the centreline), where the radial velocity v_c and the radial derivative of the axial velocity $\partial u_c/\partial r$ are both equal zero (i.e. $v_c = 0$ and $\partial u_c/\partial r = 0$):

$$u_c\frac{\mathrm{d}u_c}{\mathrm{d}x} = -\frac{\mathrm{d}p}{\mathrm{d}x} + \left(\frac{1}{r}\frac{\partial}{\partial r}\left(r\frac{\partial u}{\partial r}\right)\right)_c. \tag{3.1}$$

Then, a second equation was obtained by Langhaar by integrating the momentum equation (2.1) over the duct cross-section

$$\frac{\mathrm{d}}{\mathrm{d}x}\left(\int_0^1 ru^2\mathrm{d}r\right) = -\frac{1}{2}\frac{\mathrm{d}p}{\mathrm{d}x} + \left(\frac{\partial u}{\partial r}\right)_{r=1}. \tag{3.2}$$

Comparing the terms that equate $\mathrm{d}p/\mathrm{d}x$ in one equation to those in the other equation, $\mathrm{d}p/\mathrm{d}x$ was eliminated and a functional form for $\mathrm{d}x/\mathrm{d}\gamma$ was obtained by Langhaar. For the purpose of determining the pressure drop, Langhaar used the mechanical-energy equation, which is equivalent to the integral method (see Sparrow, Lin & Lundgren 1964), since the mechanical-energy equation was constructed by multiplying the momentum equation (2.1) by the velocity u and integrating over the duct cross-section. By means of the continuity equation (2.2), the boundary condition (2.5) and the continuity integral equation (2.6), the mechanical-energy equation reduces

to

$$\frac{\mathrm{d}}{\mathrm{d}x}\left(\int_0^1 r\frac{u^3}{2}\mathrm{d}r\right) = -\frac{1}{2}\frac{\mathrm{d}p}{\mathrm{d}x} - \int_0^1 r\left(\frac{\partial u}{\partial r}\right)^2 \mathrm{d}r. \tag{3.3}$$

The pressure drop that was determined by Langhaar employing the above equation was in good agreement with the results of other investigations (e.g. see Sparrow *et al.* 1964; Campbell & Slattery 1963). We have summarized Langhaar's procedure here to enable comparison with our forthcoming procedure.

From the formal point of view, the pressure may be determined from either the momentum equation evaluated at the centreline (3.1) or from the momentum integral equation (3.2). In this regard, note that since the analytical solution (2.12) for the velocity u is the solution of a linearized equation and not the original, then substituting the solution for u in the above-mentioned accurate equations leads to various results for the pressure drop $\mathrm{d}p/\mathrm{d}x$, which slightly differ from each other. For example, in the case of a concentric annular duct (which is relevant to, but not, the case studied here) Shumway & McEligot (1971) showed that the pressure drop found by Heaton, Reynolds & Kays (1964), which was obtained using Langhaar's momentum integral equation, differed by 20% for $x \leqslant 10^{-3}$ from the results based on the mechanical-energy integral equation. However, this inconsistency does not detract from the value of Langhaar's classical solution, since for an initially uniform velocity profile Langhaar still has (after carrying out his linearization) two unknowns γ (or $\mathrm{d}x/\mathrm{d}\gamma$) and $(\mathrm{d}p/\mathrm{d}x)$, so he employs (3.1) and (3.2) to determine $\mathrm{d}x/\mathrm{d}\gamma$ and finally obtains a satisfactory result for $\mathrm{d}p/\mathrm{d}x$ by employing the mechanical-energy equation (3.3).

However in our case, for a non-uniform initial velocity profile, we have three unknowns: $\frac{\mathrm{d}x}{\mathrm{d}\gamma}$, $\frac{\mathrm{d}p}{\mathrm{d}x}$ and $u_{bound}(\gamma, r)$ (or the unknown function $f(\gamma)$). Hence, to use simultaneously all three auxiliary equations, namely the momentum equation at the centreline (3.1), the momentum integral equation (3.2) and the mechanical-energy equation (3.3) would require adjusting the pressure term so that the final results would be the same irrespective of what combination of the three auxiliary equations one uses.

Note that the pressure gradient term may be regarded as consisting of two parts: a constant part which is the pressure gradient for a fully developed Poiseuille flow, and a variable part which describes the deviation from the fully developed pressure gradient. In order to obtain the same results with the use of any combination of the three foregoing auxiliary equations, we introduce here a weight factor $k(\gamma)$ to the variable part of the pressure gradient. Doing this, we keep in mind that the velocity profile $u(\gamma, r)$ presented by (2.12) is a solution of the linearized equation (2.8) and not of the original momentum equation (2.1). Thus, the weight factor $k(\gamma)$ makes the results for the pressure gradient consistent when solving each of these auxiliary equations, so that the solution of each auxiliary equation reaches the fully developed Poiseuille flow at the same axial distance.

The weight factor $k(\gamma)$ may be found as follows. As mentioned above we divide the pressure gradient into two parts: a constant part and a variable part, i.e.

$$\frac{\mathrm{d}p}{\mathrm{d}x} = \left(\frac{\mathrm{d}p}{\mathrm{d}x}\right)_{const} + k(\gamma)\left(\frac{\mathrm{d}p}{\mathrm{d}x}\right)_{var}. \tag{3.4}$$

The constant part of the pressure gradient $(dp/dx)_{const}$ may be found from the momentum equation (2.1) for the Poiseuille fully developed velocity profile

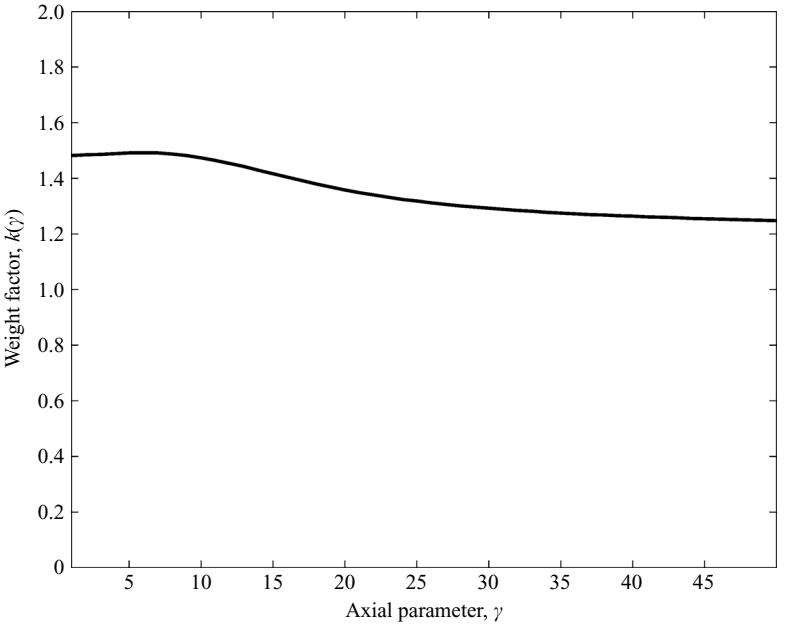

FIGURE 2. Weight factor $k(\gamma)$ for the variable part of the pressure drop (see equation (3.6)).

$u_\infty = 2(1-r^2)$ as follows:

$$\left(\frac{\mathrm{dp}}{\mathrm{d}x}\right)_{const} = \frac{1}{r}\frac{\partial}{\partial r}\left(r\frac{\partial u_\infty}{\partial r}\right) = -8. \tag{3.5}$$

Now we employ equation (3.4) in the centreline momentum equation (3.1) and the momentum integral equation (3.2).

The weight factor $k(\gamma)$ may be found after some rearrangements of (3.1)–(3.5) as

$$k = \frac{\left(4+\left(\frac{\partial u}{\partial r}\right)_{r=1}\right)u_c\frac{\mathrm{d}u_c}{\mathrm{d}\gamma} - \left(8+\left(\frac{1}{r}\frac{\partial}{\partial r}\left(r\frac{\partial u}{\partial r}\right)\right)_c\right)\frac{\mathrm{d}}{\mathrm{d}\gamma}\int_0^1 ru^2\mathrm{d}r}{\left(4-\int_0^1 r\left(\frac{\partial u}{\partial r}\right)^2\mathrm{d}r\right)\left(u_c\frac{\mathrm{d}u_c}{\mathrm{d}\gamma} - 2\frac{\mathrm{d}}{\mathrm{d}\gamma}\int_0^1 ru^2\mathrm{d}r\right) + \left(2\left(\frac{\partial u}{\partial r}\right)_{r=1} - \left(\frac{1}{r}\frac{\partial}{\partial r}\left(r\frac{\partial u}{\partial r}\right)\right)_c\right)\frac{\mathrm{d}}{\mathrm{d}\gamma}\int_0^1 r\frac{u^3}{2}\mathrm{d}r}. \tag{3.6}$$

The behaviour of the factor $k(\gamma)$ is presented in figure 2. Note that $(\mathrm{d}p/\mathrm{d}x)_{var}$, which represents the deviation of the local gradient from the fully developed pressure gradient, gradually decreases as the axial distance increases and finally vanishes on reaching the fully developed velocity profile, but the value of the factor k slightly increases, from the initial value $k = \frac{6}{5}(= 1.2)$ (for $\gamma \to \infty$) up to its final value $k = \frac{40}{27}(\approx 1.48)$ (for $\gamma \to 0$). Thus, the higher values of k multiply values of $(\mathrm{d}p/\mathrm{d}x)_{var}$ that are approaching zero.

The boundary between the accelerated and the decelerated zones of the developing flow is shown in figure 3. The accelerated zone corresponds to the centre core of the flow whereas the decelerated zone lies near the wall of a tube. Along this boundary between the decelerating and accelerating zones, the flow does not accelerate, and thus this boundary should be at the radial locations at which neutrally buoyant particles tend to concentrate. This argument is based on Soo's assertion (Soo 1990) that the 'maximum concentration (of particles) occurs where the velocity gradient is least',

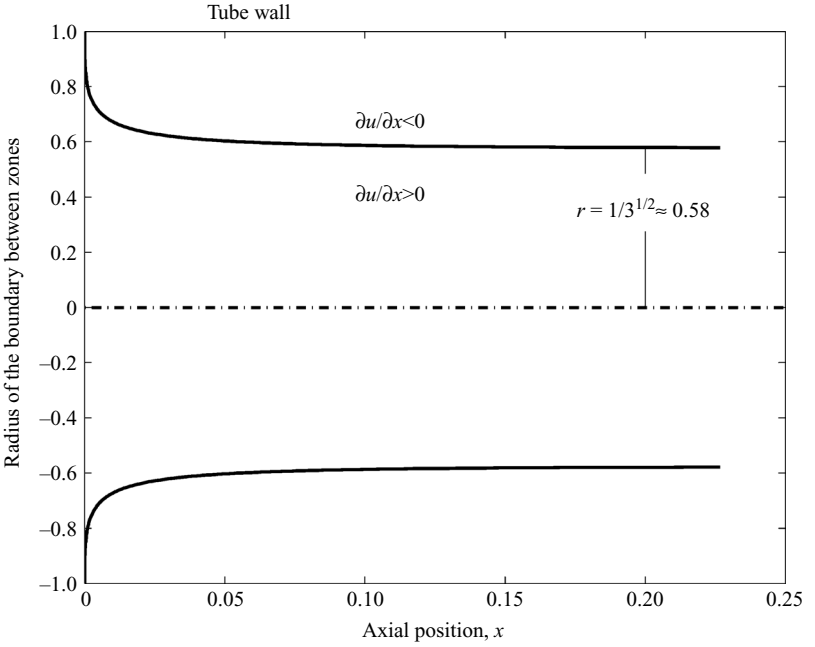

FIGURE 3. Boundary between the accelerated and the decelerated zones for a developing flow with a uniform initial velocity profile.

and is also supported by the following qualitative comparison with experimental results: Segré & Silberberg (1962) (see figure 8 on p. 152 in their paper) show the concentration of particles at various radial positions as the flow develops. The general behaviour of their results qualitatively corresponds to what we show in figure 3. The velocity u_{bound} is evaluated along this boundary.

4. Evaluation of the unknown function $f(\gamma)$: analysis and discussion of gaseous flow fields

To find the unknown function $f(\gamma)$, we use the momentum equation at the centreline in the form of (3.1), the momentum integral equation (3.2) and the mechanical-energy equation (3.3).

Combining equations (3.1) and (3.2) we obtain the derivative $\mathrm{d}x/\mathrm{d}\gamma$ as

$$\frac{\mathrm{d}x}{\mathrm{d}\gamma} = \frac{\dfrac{\mathrm{d}}{\mathrm{d}\gamma}\left(2\displaystyle\int_0^1 ru^2\mathrm{d}r - \frac{u_c^2}{2}\right)}{2\left(\dfrac{\partial u}{\partial r}\right)_{r=1} - \left(\dfrac{1}{r}\dfrac{\partial}{\partial r}\left(r\dfrac{\partial u}{\partial r}\right)\right)_{r=0}}. \tag{4.1}$$

The other form of the derivative $\mathrm{d}x/\mathrm{d}\gamma$ is obtained via combining (3.1) and (3.3) (and employing 3.4):

$$\frac{\mathrm{d}x}{\mathrm{d}\gamma} = \frac{\dfrac{\mathrm{d}}{\mathrm{d}\gamma}\left(\dfrac{u_c^2}{2} - k\displaystyle\int_0^1 ru^3\mathrm{d}r\right)}{\left(\frac{1}{r}\dfrac{\partial}{\partial r}\left(\left(r\dfrac{\partial u}{\partial r}\right)\right)_{r=0} + 2k\displaystyle\int_0^1 r\left(\left(\frac{\partial u}{\partial r}\right)\right)^2\mathrm{d}r - 8(k-1)\right)}. \tag{4.2}$$

Then, by comparing equations (4.1) and (4.2), the derivative $\mathrm{d}x/\mathrm{d}\gamma$ is eliminated and finally by substituting the velocity u from (2.12) and the weight factor k from (3.6) we obtain an equation for the function f (note that the function f appears implicitly in u, see 2.12):

$$\frac{\mathrm{d}f}{\mathrm{d}\gamma} = F(\gamma, f) \tag{4.3}$$

which is solved here numerically, satisfying the initial condition (2.13), for various spatially periodic initial velocity profiles.

Figure 4 shows the evolution of the axial velocity profiles u, calculated from equations (2.12) and (4.3), for a non-uniform initial profile $u(0, r) = 1 + \xi(r)$ (see (2.9)), where

$$\xi(r) = b\cos(4\pi r). \tag{4.4}$$

The value of γ at the inlet section of a tube is infinite. Thus, in order to obtain a starting point for our calculations the following asymptotic profile was used:

$$u_L(\gamma \gg 1) \approx \left(1 + \frac{2}{\gamma}\right)(1 - \mathrm{e}^{\gamma(r-1)}) \tag{4.5}$$

which is correct for large values of γ.

Substituting (2.12) with (4.5) into equation (4.3) and neglecting infinitesimal terms of the second order, we obtain asymptotic relations for functions $f(\gamma)$ and $x(\gamma)$ for large values of γ in the form

$$f(\gamma \gg 1) = 1 - \frac{k_f(b)}{\gamma} \tag{4.6}$$

and

$$x(\gamma \gg 1) = \frac{k_x(b)}{\gamma^2}, \tag{4.7}$$

where the constant coefficients $k_f(b)$ and $k_x(b)$ depend on the amplitude b (see (4.4)).

Taking into account that the axial position x must be positive, we obtain from (4.7) an allowable range for values of b:

$$-0.71 < b < 0.18. \tag{4.8}$$

The above closed forms of the above coefficients were obtained with the aid of *Mathematica*, the system for symbolic calculations (Wolfram 1991).

Setting a certain large initial numerical value for γ, we obtain an initial value for the function $f(\gamma)$ employing (4.6) and then the process of calculation starts.

Next, the relationship between x and γ may be found from (4.1) or (4.2), and the pressure gradient $\mathrm{d}p/\mathrm{d}x$ can be found by employing (3.3).

The radial velocity component v may be obtained from the continuity equation (2.2) using the following formula (Ulrichson & Schmitz 1965):

$$v = -\frac{1}{r}\frac{\mathrm{d}}{\mathrm{d}\gamma}\left(\int_0^r ru\mathrm{d}r\right) \Big/ \left(\frac{\mathrm{d}x}{\mathrm{d}\gamma}\right). \tag{4.9}$$

The downstream evolution of the velocity profiles is presented in figure 4 at the following downstream locations: $x = 0.0025; 0.01; 0.04; 0.16$ (note that γ is related to the downstream distance x through equation (4.1)) for various initial profiles defined by different b values: $b = 0.12; 0.07; -0.18; -0.37$, see cases (*a*), (*b*), (*c*) and (*d*), respectively, where each b represents the wave-shape amplitude. Note that the initial

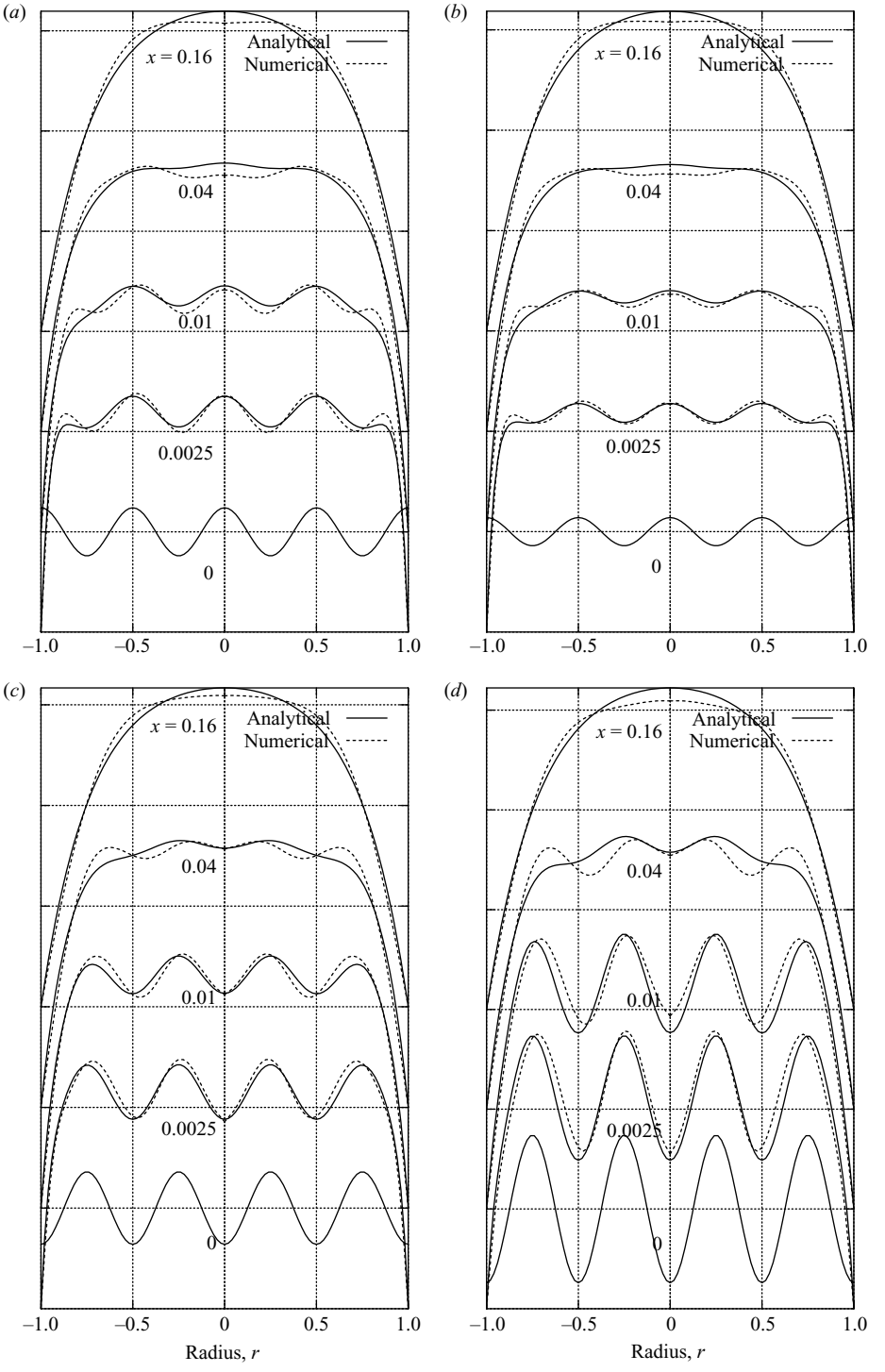

FIGURE 4. Downstream evolution of the developing velocity profiles for four different initial conditions of a gaseous flow in a circular tube: (a) $b = 0.12$, (b) $b = 0.07$, (c) $b = -0.18$, (d) $b = -0.37$. Note that the initial velocity profiles in (a) and (b) are characterized by a velocity peak in the centre of the tube, whereas in cases (c) and (d) the initial velocity peaks are off the tube centre.

velocity profiles (a) and (b) are characterized by a velocity peak in the centre of the tube, whereas in cases (c) and (d), the initial velocity peak is off the tube centre.

One can see, as expected, that for spatially periodic initial velocity distributions the influence of fast and slow zones of the flow is counterbalanced owing to their interaction. When the amplitude b approaches small values, e.g. $b = 0.07$, the downstream profiles already resemble the profiles that evolve from a uniform initial velocity distribution. Langhaar's results are fully reproduced when we substitute $b = 0$ in our solution.

In order to validate our solutions for the host-gas flow, we employed the Nekhamkina & Rotinjan (1978) numerical code. This code was constructed to solve viscous boundary-layer equations of a single phase, e.g. air without droplets, in which the pressure is assumed constant in the lateral direction, and is capable of handling an initial non-uniform velocity profile. This code is based on an approach suggested by Patankar & Spalding (1967), when a stream function is introduced and the system of nonlinear finite-differences equations is solved by iterations. This numerical code was tested by comparison of its results with other numerical solutions (Hornbeck 1964; Liu 1974; see also Shah & London 1978, Table 10). The difference between results was less than 0.5%.

The term 'validation' is usually reserved for the process of ensuring that the equations solved describe the physical reality, i.e. agreement with experimental observations. However, since we have linearized the original governing equations which for decades have agreed with the observed physical reality of viscous flows, we should check whether our linearization of the original equations still captures the physical reality.

In this regard, as can be seen in figure 4, the velocity profiles that evolve from the four different spatially periodic initial velocities not only conserve the qualitative physical behaviour but also quantitatively show that the deviations of our analytical solution of the linearized equations from the numerical solution of the original viscous flow equations are minor (about 1%) for most radial positions along the tube flow field and reach a maximum of about 4% deviation at some local peaks of the flow velocity where the linearized equations tend to relax these peaks somewhat faster than the original equations. This behaviour is expected since this is usual for local linearization of nonlinear terms. Thus, the present validation provides strong support for the physical underpinning of our modified linearization procedure.

Figure 5 shows that the velocities at the centreline for different initial profiles become almost the same after a short distance $x \approx 0.02$. Therefore, all such profiles approach the Poiseuille fully developed profile at downstream distances which are very close to each other. Note that in Langhaar's solution, the Poiseuille developed flow is obtained when $\gamma \to 0$, i.e. when $x \to \infty$. However for $\gamma \approx 0.7$ (and $x \approx 0.227$) the maximal velocity of the present 'developed flow' deviates by less than 1% from Poiseuille's maximum velocity.

In the new solutions presented here, we employ the function $f(x)$ (or $f(\gamma)$). It is interesting to observe the behaviour of the function f for various b values (b defines the amplitude of the spatially periodic initial profile), as presented in figure 6. Note, that when the function f reaches zero, the velocity profile turns into the classical Langhaar's profile, see equation (2.12). This happens at small γ values which are equivalent to large x values. This relationship between the axial position x and Langhaar's function γ is shown in figure 7 for various b values, and is almost identical for each profile which initially has a spatially periodic shape.

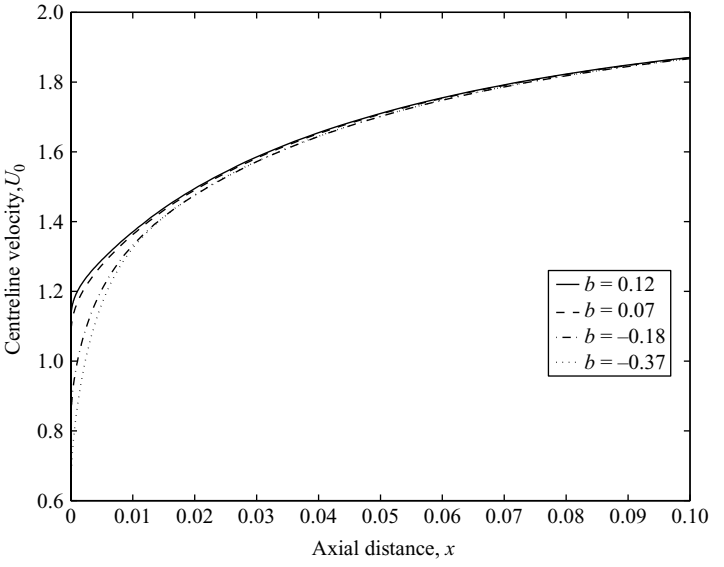

FIGURE 5. Velocity at the centreline of the tube for various values of b (b defines the form and the amplitude of the initial spatially periodic velocity profile).

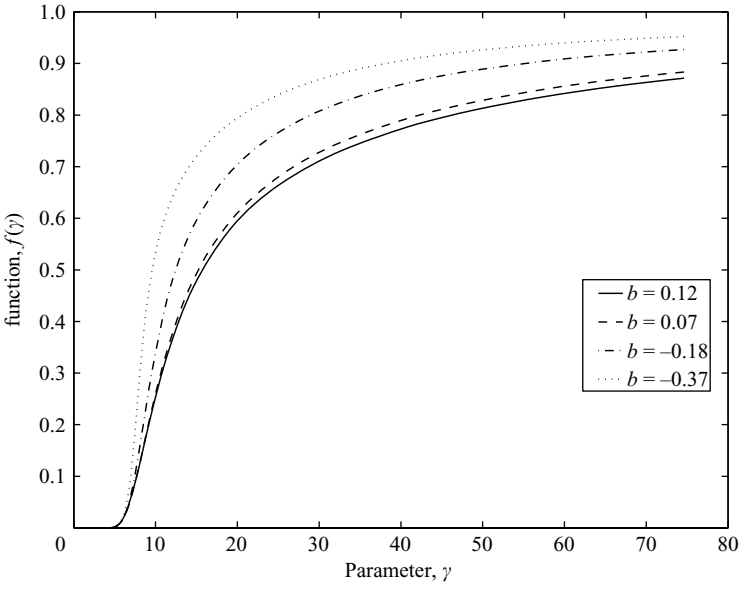

FIGURE 6. Auxiliary function $f(\gamma)$ for various b values.

Figure 8 shows the influence of the initial profile on the non-dimensional pressure drop in the downstream direction. In the fully developed flow region, the pressure gradient approaches a constant value (see equation (3.5)), and the pressure drop between the inlet section and the downstream locations rises linearly. However, the pressure gradient in the developing flow region near the inlet is steeper than that in the fully developed flow, so an excess pressure drop is formed. This pressure drop at the entrance region, sometimes called the 'Hagenbach factor', is of great interest in

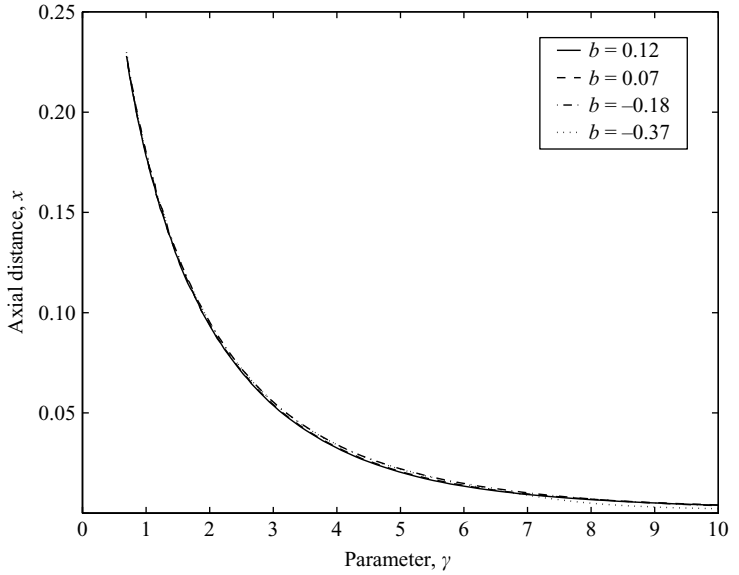

FIGURE 7. The relationship between the axial position x and Langhaar's function γ for various b values.

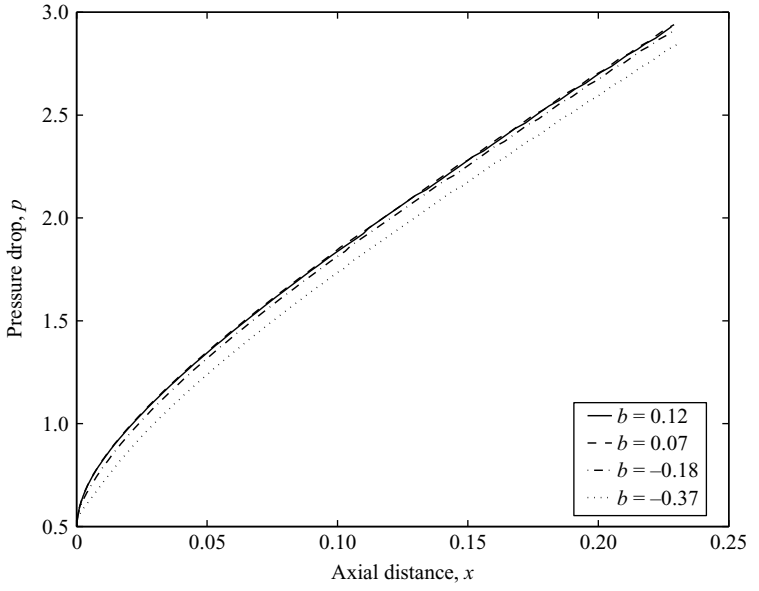

FIGURE 8. The relationship between the normalized pressure drop p and the downstream distance x from the tube inlet for various b values.

classical fluid mechanics. Langhaar (1942), Sparrow *et al.* (1964) and other authors widely discussed this issue for a uniform initial velocity profile and revealed two distinct contributions, made by: (i) the change in momentum and energy between the initial and the developing velocity profiles; (ii) the large frictional losses of the developing flow relative to the Poiseuille flow. The final value of the first contribution shows the pressure drop necessary to accelerate a flow into a fully developed Poiseuille

profile, and is equal $\frac{2}{3}$ when the initial velocity profile is uniform. However, for a non-uniform initial profile (equation (4.4)), this becomes $(\frac{2}{3} - b^2)$. Hence, a symmetrical spatially periodic velocity profile like those described by equation (4.4) with a larger amplitude requires less force and energy to be accelerated into a fully developed profile than a more uniform initial profile. Thus, as is shown in figure 8, the lines related to the larger b values lie below those for smaller b values.

In the next sections, the velocity fields of non-evaporating and evaporating droplets will be analysed. Since the gas-phase velocity and the droplets velocity field are mutually coupled our modified linearization will be employed for the momentum equation of each of the phases, namely the host-gas phase and the liquid phase (droplets).

5. Non-evaporating droplets suspended in a developing initially uniform flow

We begin by analysing a monosize population of non-evaporating liquid droplets (or particles). Droplets that are introduced into the moving gas initially have a velocity which differs from the velocity of the host gas. During the motion of the droplets, their velocity gradually approaches the velocity of the host gas, due to drag forces. The drag force considered in the present study is proportional to the relative velocity $(u - u_d)$ in the case of a negligible radial velocity component, as will be discussed below (see also Tambour & Zehavi 1993).

The droplet flow field may be divided into two regions. The first region lies very close to the inlet of a tube where the relative velocity between the two phases is high and hence the droplet velocity changes fast. At the second region, droplets have a velocity that is close to the velocity of the host gas, and these two velocity fields gradually approach each other. We assume that in the second region, droplets move almost with the streamlines of the host gas in a tube.

First we analyse here the initial stage of droplet motion. Because of inertia, the droplet trajectories do not coincide with the streamlines of the host fluid and 'the substantial derivatives' for droplets and the host gas will be different.

The dimensionless governing equations of motion which are mutually coupled are host-gas flow

$$\frac{\mathrm{D}u}{\mathrm{D}t} = -\frac{\mathrm{d}p}{\mathrm{d}x} + \frac{1}{r}\frac{\partial}{\partial r}\left(r\frac{\partial u}{\partial r}\right) + K\varepsilon(u_d - u), \tag{5.1}$$

droplets

$$\frac{\mathrm{D}u_d}{\mathrm{D}t} = K(u - u_d), \tag{5.2}$$

where u is the host-gas flow velocity, u_d is the velocity of droplets, $\rho = \rho_d/\rho_f$ is the relative density of droplets and the host fluid, $K = 18a^2/(\rho d^2)$ is the droplet drag coefficient, a is the radius of the tube, d is a droplet diameter, and ε is mass concentration of the liquid phase (i.e. droplets). Note that the kinematic viscosity does not appear in K since it is embedded in the normalized radial velocity, axial distance and time (see the notation below equation (2.2)).

The above analytical treatment of the two-way coupling between the velocity fields of the two phases (i.e. particles or droplets and the host gas) was first presented by Saffman (1962) and Marble (1963), and was also employed in more recent studies, e.g. Tambour & Zehavi (1993), Miller & Bellan (1999) and Varanasi, Clack & Miller (2004), in which the two-way coupling between the phases was fully incorporated, in a two-dimensional simulation.

The radial velocity component v equals zero across the inlet section. Hence, at the first stage that lies close to the tube inlet, the radial velocity component still remains negligible relative to the axial velocity component. Under this assumption the equations of motion (5.1) and (5.2) may be expressed in the following form, respectively: host-gas flow

$$u\frac{\mathrm{d}u}{\mathrm{d}x} = -\frac{\mathrm{d}p}{\mathrm{d}x} + \frac{1}{r}\frac{\partial}{\partial r}\left(r\frac{\partial u}{\partial r}\right) + K\varepsilon(u_d - u), \tag{5.3}$$

droplets

$$u_d\frac{\mathrm{d}u_d}{\mathrm{d}x} = K(u - u_d). \tag{5.4}$$

Solutions are derived here for low droplet concentrations, i.e. $\varepsilon \ll 1$. For such a case, the velocity u and velocity u_d may be expanded as

$$u = u_0 + \varepsilon u_1 + \varepsilon^2 u_2 + \ldots, \tag{5.5}$$

$$u_d = u_{d,o} + \varepsilon u_{\mathrm{d},1} + \varepsilon^2 u_{d,2} + \ldots \tag{5.6}$$

Substituting (5.5) and (5.6) into (5.3) and (5.4) and comparing the terms free of ε, we obtain the following set of equations for the zeroth order of the solution:

$$u_0\frac{\mathrm{d}u_0}{\mathrm{d}x} = -\frac{\mathrm{d}p}{\mathrm{d}x} + \frac{1}{r}\frac{\partial}{\partial r}\left(r\frac{\partial u_0}{\partial r}\right), \tag{5.7}$$

$$u_{d,0}\frac{\mathrm{d}u_{d,0}}{\mathrm{d}x} = K(u_0 - u_{d,0}). \tag{5.8}$$

The corresponding initial and boundary conditions are

$$u_0(x = 0, r) = 1, \tag{5.9}$$

$$u_0(x > 0, r = 1) = 0, \tag{5.10}$$

$$\int_0^1 r u_0 \mathrm{d}r = \frac{1}{2}, \tag{5.11}$$

$$u_{d,0}(x = 0, r) = u_d(0). \tag{5.12}$$

In order to solve (5.7) we apply our modified linearization (2.8) to (5.7):

$$u_0\frac{\mathrm{d}u_0}{\mathrm{d}t} = \gamma^2(u_0 - u_{bound}) \tag{5.13}$$

and we obtain

$$u_0 = \frac{I_0(\gamma) - I_0(\gamma r)}{I_2(\gamma)}. \tag{5.14}$$

Next, we divide (5.8) by (5.13) and obtain

$$u_{d,0}\frac{\mathrm{d}u_{d,0}}{\mathrm{d}\gamma} = K\frac{u_0 - u_{d,0}}{\gamma^2(u_0 - u_{bound})}\frac{\mathrm{d}u_0}{\mathrm{d}\gamma}u_0 \tag{5.15}$$

with initial condition (5.12).

One can see now that if Langhaar's classical linearization (i.e. in the absence of the term u_{bound}) is used in (5.13) and (5.15), then the sign of the derivative $\mathrm{d}u_{d,0}/\mathrm{d}\gamma$ depends on the sign of the derivative $\mathrm{d}u_0/\mathrm{d}\gamma$. But in reality, the sign of the derivative $\mathrm{d}u_{d,0}/\mathrm{d}\gamma$ depends on the sign of the relative velocity $(u_0 - u_{d,0})$ only. This contradiction is resolved by applying our modified linearization that includes the boundary velocity

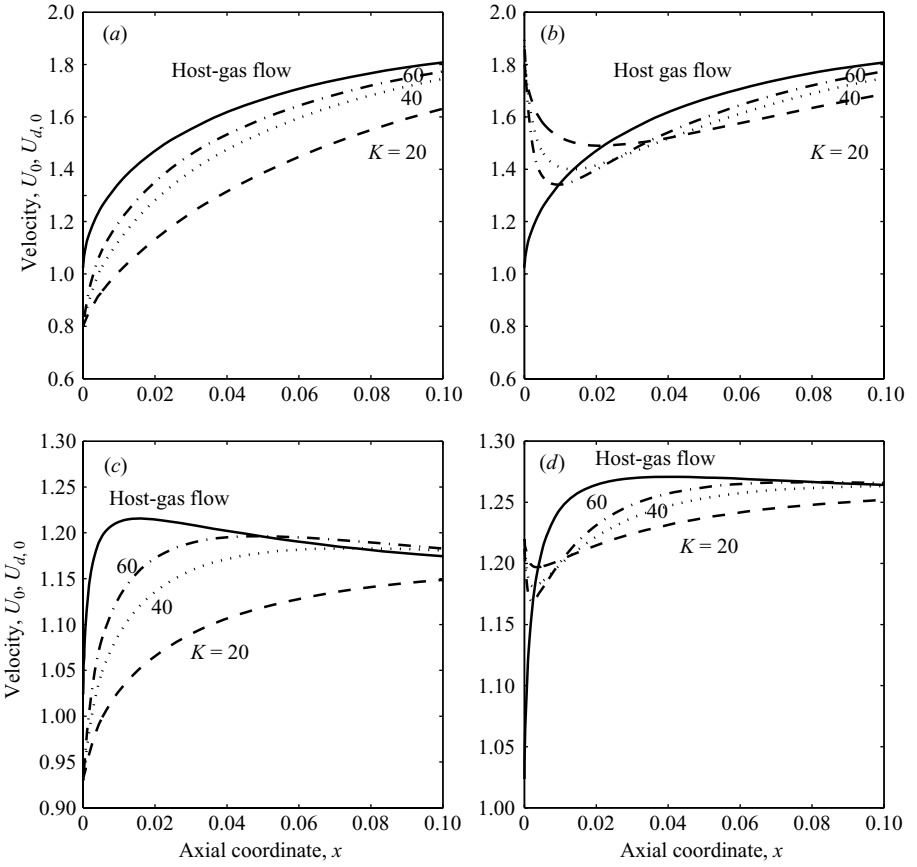

FIGURE 9. Droplet velocities in a developing tube flow. No evaporation. (*a*) Accelerating flow ($r/a = 0.2$) and accelerating droplets. (*b*) Accelerating flow ($r/a = 0.2$) and initially decelerating droplets. (*c*) Accelerating and then decelerating flow ($r/a = 0.65$) and accelerating droplets. (*d*) Accelerating and then decelerating flow ($r/a = 0.61$) and initially decelerating droplets.

u_{bound} (see (2.8) and (5.13)), because here the terms $(u_0 - u_{bound})$ and $\mathrm{d}u_0/\mathrm{d}\gamma$ have the same sign as follows from the definition of the velocity u_{bound}, see (2.17).

Equation (5.15) is an ordinary nonlinear differential equation and is integrated here numerically satisfying the initial condition given by (5.12). The results of our calculations are presented in figure 9.

Near the entrance, in the early entry region, i.e. for $\gamma \gg 1$, equation (5.14) reduces to

$$u_0 \approx 1 + \frac{2}{\gamma}, \tag{5.16}$$

and from the definition of u_{bound} one can show that (see (2.17))

$$u_{bound} \approx 1 + \frac{5/3}{\gamma}. \tag{5.17}$$

Thus, near the entrance, equation (5.15) may also be solved analytically to yield

$$u_{d,0} = \begin{cases} 1 + 4K/\gamma^3 & \text{if } u_d(0) = 1 \\ 1 - [1 - u_d(0)]\exp(-3K/\gamma^2) & \text{if } u_d(0) \neq 1 \end{cases} \tag{5.18}$$

As one can see from the above consideration and calculated results for the flow and droplet motion (figure 9), the velocity of droplets approaches the velocity of the main flow in a relatively short distance. This means that, after a short first stage, the velocity of the droplets is close to the flow velocity, and thus in the second stage the following relation may be used:

$$u_d \approx u. \tag{5.19}$$

Consider now the second stage of droplet motion. Taking into account relation (5.19) and following Saffman's method (Saffman 1962) we rewrite (5.1) and (5.2) in the following form, respectively:

$$\frac{\mathrm{D}u}{\mathrm{D}t} = -\frac{\mathrm{d}p}{\mathrm{d}x} + \frac{1}{r}\frac{\partial}{\partial r}\left(r\frac{\partial u}{\partial r}\right) + K\varepsilon(u_d - u) \tag{5.20}$$

and

$$\frac{\mathrm{D}u}{\mathrm{D}t} \approx \frac{\mathrm{D}u_d}{\mathrm{D}t} = K(u - u_d). \tag{5.21}$$

Combining (5.20) and (5.21) we can eliminate the droplet velocity u_d and obtain the equation of fluid motion as follows:

$$(1+\varepsilon)\frac{\mathrm{D}u}{\mathrm{D}t} = -\frac{\mathrm{d}p}{\mathrm{d}x} + \frac{1}{r}\frac{\partial}{\partial r}\left(r\frac{\partial u}{\partial r}\right). \tag{5.22}$$

Equation (5.22) can now be linearized in perfect analogy with our previous linearization (see (2.8)), i.e.

$$(1+\varepsilon)\frac{\mathrm{D}u}{\mathrm{D}t} = \gamma^2(u - u_{bound}), \tag{5.23}$$

whose solution for the case of an initially uniform velocity distribution is identical to (2.7):

$$u = \frac{I_0(\gamma) - I_0(\gamma r)}{I_2(\gamma)}. \tag{5.24}$$

Then the function γ is determined from the momentum equation (5.22) evaluated at the centreline and from a momentum integral equation.

As shown earlier, the first stage of droplet motion is much shorter than the second one. Hence, the relationship between the axial position x and the function γ may be rewritten for the whole region as follows:

$$x = (1+\varepsilon)\int_{\infty}^{\gamma} h(\gamma)\mathrm{d}\gamma \tag{5.25}$$

where the function $h(\gamma)$ is determined similarly to (4.1) as

$$h(\gamma) = \frac{\dfrac{\mathrm{d}}{\mathrm{d}\gamma}\left(2\displaystyle\int_0^1 ru^2\mathrm{d}r - \frac{u_c^2}{2}\right)}{2\left(\dfrac{\partial u}{\partial r}\right)_{r=1} - \left[\dfrac{1}{r}\dfrac{\partial}{\partial r}\left(r\dfrac{\partial u}{\partial r}\right)\right]_{r=0}}. \tag{5.26}$$

Equation (5.25) indicates that in the presence of droplets the development of the flow is decelerated by the factor $(1+\varepsilon)$.

The velocity of droplets u_d in the second stage may be obtained by comparison of (5.21) and (5.23), leading to the relation

$$u_d = u - \frac{\gamma^2(u - u_{bound})}{(1+\varepsilon)K}. \tag{5.27}$$

Both previously considered stages of droplet motion have a matching value for γ, for which the velocities of droplets at each stage are equal at the transition point. If the droplet drag coefficient K is large, then (5.18) may be used to calculate the droplet velocity in the first stage. For example, let the following values of parameters be specified:

$$u_d(0) = 1; \quad \varepsilon = 0.35; \quad K = 60. \tag{5.28}$$

By using (5.16)–(5.18) and (5.27) we obtain the matching value $\gamma_{transition}$ to be

$$\gamma_{transition} \approx 9.5. \tag{5.29}$$

This means that for the conditions chosen in the above example, the matching point lies very close to the inlet (see figure 7).

6. Evaporating droplets suspended in a developing initially uniform flow

Next, we consider the changes in the value of the droplet drag coefficient due to the decrease in droplet diameter as a result of droplet evaporation. According to the d^2 -law of evaporation:

$$\frac{\mathrm{d}(d^2)}{\mathrm{d}t} = -E \tag{6.1}$$

where E is the evaporation coefficient.

Taking into account the relationship between the droplet diameter d and the drag coefficient K

$$d^2 = \frac{18a^2}{\rho}\frac{1}{K} \tag{6.2}$$

and substituting the above equation into (6.1), we obtain

$$\frac{\mathrm{d}(1/K)}{\mathrm{d}t} = -\frac{E\rho}{18a^2}. \tag{6.3}$$

Replacing $\mathrm{d}t$ by $\mathrm{d}x/u_{d,0}$, then replacing $\mathrm{d}x$ by $((\mathrm{d}x/\mathrm{d}\gamma)\mathrm{d}\gamma)$ and accordingly transforming equation (6.3), we obtain

$$\frac{\mathrm{d}(1/K)}{\mathrm{d}\gamma} = -\frac{E\rho}{18a^2}\frac{1}{u_{d,0}}\frac{\mathrm{d}x}{\mathrm{d}\gamma}. \tag{6.4}$$

Equation (6.4) may now be added to equation (5.15) and solved numerically.

Next, we treat the case of $\gamma \gg 1$. We solve (6.4) for $u_{d,0} = 1$ and $\gamma \gg 1$. Employing (4.1) in which we use $\gamma \gg 1$, we obtain

$$\frac{\mathrm{d}x}{\mathrm{d}\gamma} \approx -\frac{1}{2\gamma^3}. \tag{6.5}$$

Substituting (6.5) into (6.4) and solving the resulting equation, we obtain an expression for the drag coefficient K as a function of its initial value K_0,

$$K \approx K_0\left(1 + \frac{K_0 E\rho}{18a^2}\frac{1}{4\gamma^2}\right). \tag{6.6}$$

Using equations (5.16), (5.17) and (6.6) in (5.15), we obtain the development of the droplets velocity in the early region, in which evaporation of droplets is accounted for,

$$u_{d,0} = 1 + \frac{4K_0}{\gamma^3} + \frac{6K_0}{\gamma^4} + \frac{3K_0^2}{5\gamma^5}\left(\frac{E\rho}{18a^2} - 8\right) \tag{6.7}$$

under the initial condition $u_d(0) = 1$.

As was mentioned earlier, after a short initial stage, the velocities of non-evaporating droplets become close to the host-flow velocity. In the case of evaporating droplets, the droplets moving with the flow become smaller and then disappear releasing vapour which propagates in the tube due to diffusion and convection. Our purpose now is to determine the concentrations of the evaporating droplets and the production of vapour in the tube. The non-dimensional governing equations of motion obtained according to the d^2-law of evaporation (see Tambour 1984, 1985; Katoshevski & Tambour 1993) are
for the evaporating droplets

$$u\frac{\partial m_d}{\partial x} + v\frac{\partial m_d}{\partial r} = -\bar{E}m_d^{1/3}, \tag{6.8}$$

and for the vapour

$$u\frac{\partial m}{\partial x} + v\frac{\partial m}{\partial r} = \frac{D}{r}\frac{\partial}{\partial r}\left(r\frac{\partial m}{\partial r}\right) + \bar{E}m_d^{1/3}, \tag{6.9}$$

where $m_d = (\mathrm{d}/\mathrm{d}_0)^3$ is the mass of a droplet, related to its initial mass, $m_d(0) = \frac{1}{6}\pi\rho_d d_0^3$ is the initial droplet mass, d_0 is the initial droplet diameter, d is the instantaneous droplet diameter, $m = m_{vapor}/m_d(0)$ is mass of produced vapour, related to the initial droplet mass, D is diffusion coefficient, and $\bar{E} = 3Ea^2/(2\pi d_0^2 \nu)$ is non-dimensional evaporation coefficient.

It is difficult to treat equations (6.8) and (6.9) analytically because some droplets vanish due to the evaporation process at different points in a tube depending on their trajectories, and we cannot allow a negative droplet mass.

Because of this, equations (6.8) and (6.9) were solved numerically, for different values of the evaporation coefficient $\bar{E}$. Velocities u and v were calculated by employing equations (5.24) and (4.9), respectively.

The boundary conditions are determined by symmetry

$$\left.\frac{\partial m}{\partial r}\right|_{r=0} = 0 \tag{6.10}$$

and by the non-permeability condition at the tube wall

$$\left.\frac{\partial m}{\partial r}\right|_{r=1} = 0. \tag{6.11}$$

Initial conditions are determined by the uniform distribution of droplets in the duct inlet section

$$m_d(x = 0, r) = 1 \tag{6.12}$$

and by the absence of vapour in this section

$$m_d(x = 0, r) = 0. \tag{6.13}$$

The results of our calculations were checked by the mass balance relation which was obtained after integrating equations (6.8) and (6.9) over the tube cross-section,

with the use of the boundary conditions (6.10) and (6.11):

$$\frac{\mathrm{d}}{\mathrm{d}x}\int_0^1 (m_\mathrm{d}+m)ur\,\mathrm{d}r = 0. \tag{6.14}$$

Concentration profiles of the droplet phase and the vapour phase are shown below in figures 11 and 12, respectively.

7. Results and discussion of the droplet flow field

A schematic description of the problem is presented in figure 1. We treat here: (i) flows developing from spatially periodic initial velocity distributions without the presence of droplets, see figure 1(*a*), (already presented and discussed in §4), and (ii) two-phase flows in which monosize, nonevaporating and evaporating droplets suspended in a developing gas flow of an initially uniform velocity distribution exchange momentum with the host-gas flow, see figure 1(*b*) discussed below.

The behaviour of droplets suspended in a duct flow developing from an initially uniform velocity profile is presented in figure 9. One can see a few 'modes' of the relative motion of the droplets and the flow. Figures 9(*a*) and 9(*b*) show the relative motion of the droplets and the flow in the region of an accelerating flow. We have chosen two radial locations, one at the central 'inner' region ($0 \leqslant r < 0.58$) presented in figures 9(*a*) and 9(*b*), and the other within the 'outer' region $0.58 \leqslant r < 1$ in figures 9(*c*) and 9(*d*). Note that there is a fundamental difference between these two regions in the host-gas flow behaviour. In the inner region, the flow accelerates, whereas in the outer region, the flow accelerates initially and then decelerates (see figure 9).

Two particular cases are presented here: one for an initial droplet velocity which is lower than the initial host-gas velocity, and the second for an initial droplet velocity which is higher than the initial host-gas velocity. The motion of droplets which start with initial velocity $u_{d,0}$ lower than the initial gas velocity ($u_{d,0} < 1$) is presented in figure 9(*a*). One can see that all droplets are gradually accelerated and their velocities eventually approach the fluid velocity. Smaller droplets with higher drag coefficients (higher values of K) are subject to a larger acceleration and their velocity reaches the flow velocity faster (i.e. in a shorter distance). When the initial droplet velocity is higher than the initial flow velocity ($u_{d,0} > 1$) (see figure 9*b*), the droplets decelerate up to the moment at which their velocity reaches the velocity of the flow. Then they start to accelerate but lag behind the velocity of the host gas. Note that as expected the smaller droplets approach the flow velocity faster.

The behaviour of droplets in the outer region of the tube is presented in figures 9(*c*), 9(*d*). This is the region between $r \approx 0.58$ and the wall, $r = 1$ (for an exact definition, see figure 3). In this region, the flow velocity increases initially and then begins to decrease, because (at a certain axial position) the boundary layer reaches this position and makes the flow decelerate.

When the initial droplet velocity is smaller than the flow velocity ($u_{d,0} < 1$), the large droplets (of a low drag coefficient) are accelerated slowly and their velocity finally approaches the flow velocity (see figure 9*c*, $K = 20$). The velocity of small droplets reaches the flow velocity and even exceeds its value when the host-gas velocity decelerates. Then eventually the droplet velocity approaches the flow velocity from above.

The motion of droplets with high initial velocities ($u_{d,0} > 1$) (see figure 9*d*) may be described as a combination of the two last cases (figures 9*b* and 9*c*). Here there is

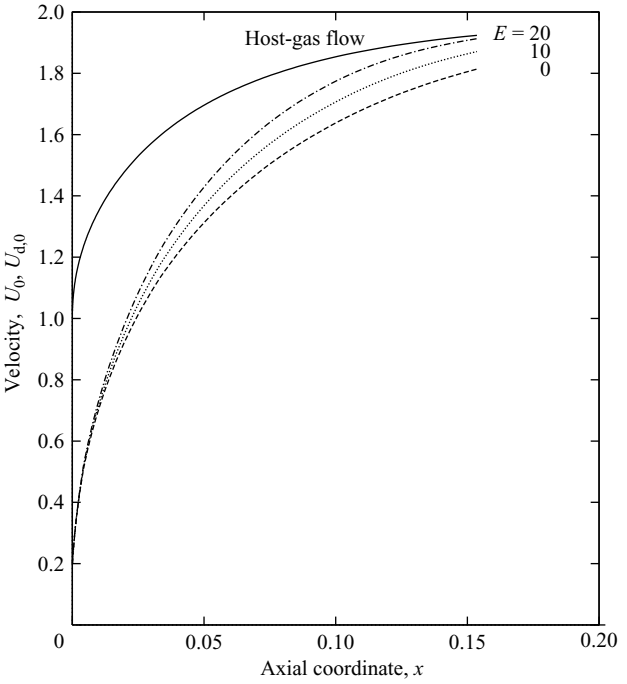

FIGURE 10. Droplet velocities in a developing tube flow. Evaporation is present. Accelerating flow ($r/a = 0.1$) and accelerating droplets. The rate of evaporation is determined by E, see equation (6.1).

initially an interaction between a slow flow and fast droplets and followed by a fast flow which accelerates slow droplets.

Note that when evaporation is present, droplets become smaller and thus the drag coefficient increases. Hence the behaviour of evaporating droplets will be transitional, i.e. it will shift from the behaviour of large droplets to the behaviour of smaller droplets (see figure 10).

Figure 11 shows the mass distribution of droplets which was calculated from equation (6.8), for different values of non-dimensional evaporation coefficient $\bar{E}$. The total mass of the droplets over each cross-section of the tube decreases with increasing downstream distance. The region where the droplets may be found also decreases. Enhancement of $\bar{E}$ accelerates these processes, but the differences between the amounts of liquid phase for various evaporation rates become significant only far from the tube inlet (see for comparison figures 11*a*, 11*b* and 11*c*). Another effect is that in the central core of the tube, the distribution of the liquid phase is nearly uniform, and a severe decrease in the droplet concentration is observed near the edge of the zone where the droplets exist, due to the longer residence time of the droplets.

Dispersion of vapour produced by evaporation of moving droplets is shown in figure 12, for various levels of evaporation rate $\bar{E}$. Initially the more intensive evaporation process is observed near the tube wall, where the droplet velocity is small and the residence time of the droplets in this zone is large. When the droplets move further downstream, the process of diffusion leads to equalization of vapour concentration. However, the zone of intensive evaporation shifts toward the tube centreline, because the droplets near the wall vaporize completely (see figure 11). As a result, one can see a peak of vapour concentration far from the tube wall (see line $x = 0.122$ in figure 12*a*

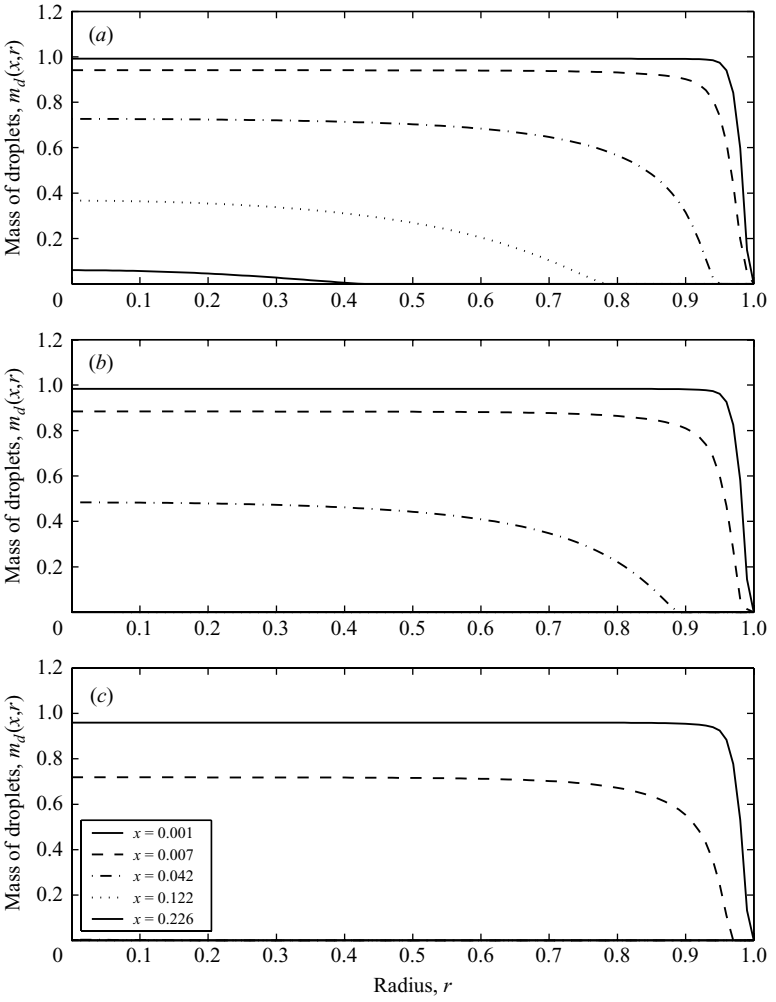

FIGURE 11. Lateral and axial evolution of mass concentration of the liquid phase (evaporating droplets) across the tube for various evaporation rates; $\bar{E}$ is the normalized evaporation coefficient. (*a*) $\bar{E} = 10$, (*b*) $\bar{E} = 20$, (*c*) $\bar{E} = 50$.

and line $x = 0.042$ in figure 12*b*). The enhancement of evaporation rate leads to faster complete evaporation of droplets and hence the pure vapour phase is obtained at a shorter downstream distance from the duct inlet. This vapour is exposed to mass transfer due to dispersion, i.e. the simultaneous influence of diffusion and flow. The dispersion leads to equalization of vapour concentration over the cross-section of the tube, and finally this concentration becomes uniform (at the end of the entrance region, see lines $x = 0.122$ and $x = 0.226$ in figures 12*b* and 12*c*).

8. Concluding remarks

In conclusion, a new approach has been presented for the analysis of developing non-uniform spatially periodic flows in the entrance region of ducts. The theoretical predictions of the evolution of spatially periodic velocity profiles have been validated by numerical calculations. This provides strong support for the physical underpinnings

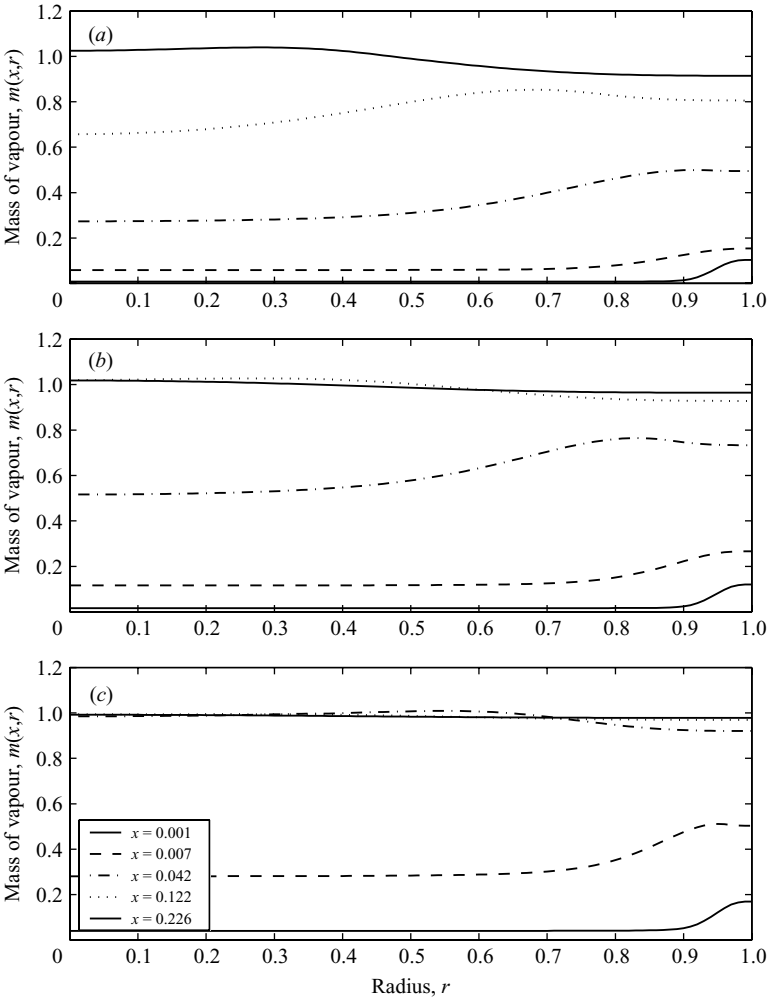

FIGURE 12. Effect of various rates of evaporation on vapour distribution across and along the tube. (*a*) $\bar{E} = 10$, (*b*) $\bar{E} = 20$, (*c*) $\bar{E} = 50$.

of the present modified linearization procedure. Thus, it is possible to extend the present solution to a variety of flows in which the initial velocity distribution may be regarded as consisting of periodic spatial distributions having different characteristic frequencies. For an initially uniform developing flow, the present modified linearization enables us to treat here the dynamics of non-evaporating and evaporating droplets. Asymptotic solutions have been presented for the flow region which lies very close to the inlet of the tube in which the relative velocity between the droplets and the host gas is high, and thus the velocity fields of the two phases are mutually coupled. These solutions provide new explicit formulae for the droplet velocity field as a function of the initial conditions and droplet diameter (relative to the tube diameter) for non-evaporating drops (equations (5.18), (5.27)), and also a function of evaporation rate (equation (6.7)) for evaporating drops. Thus, for a given duct flow and known vaporization rates, one can determine the desired size of droplets so that drop velocities would reach the host-gas velocity within desired distances of the entrance region.

S.K. is grateful to Dr O. Nekhamkina for allowing him to use her numerical code. Y. T. is grateful to the Stephen E. Berger Chair endowment.

REFERENCES

Anidjar, F., Greenberg, J. B. & Tambour, Y. 1996 On the solution of a class of polydisperse spray problems. *Eur. J. Appl. Maths.* **7**, 75–96.

Asmolov, E. S. 1999 The inertial lift on a spherical particle in a plane Poiseuille flow at large channel Reynolds number. *J. Fluid Mech.* **381**, 63–87.

Berestycki, H. & Sivashinsky, G. I. 1991 Flame extinction by periodic flow field. *SIAM J. Appl. Maths* **55**, 344–350.

Borghi, R. 1996 Background on droplets and sprays. In *Combustion and Turbulence in Two-phase Flows*. Lecture series 1996-02. Von Karman Institute of Fluid Dynamics.

Campbell, W. D. & Slattery, J. C. 1963 Flow in the entrance of a tube. *Trans. ASME: J. Basic Engng* **85**, 41–46.

Candel, S., Lacas, F., Darabiha, N. & Rolon, C. 1999 Group combustion in spray flames. *Multiphase Sci. Tech.* **11**, 1–18.

Chigier, N. & Gemci, T. 2002 Problems and challenges in the development of micro-propulsion devices. In *Proc. 42nd Israel Conf. on Aerospace Sciences,* Technion-Israel Institute of Technology, Haifa, Israel.

Greenberg, J. B. & Cohen, R. 1992 Spatial distortion of spray diffusion flames. *Atomization Spray* **2**, 275–293.

Heaton, H. S., Reynolds, W. C. & Kays, W. M. 1964 Heat transfer in annular passages: simultaneous development of velocity and temperature fields in laminar flow. *Intl J. Heat Mass Transfer* **7**, 763–781.

Hornbeck, R. W. 1964 Laminar flow in the entrance region of a pipe. *Appl. Sci. Res.* A **13**, 224–232.

Katoshevski, D. & Tambour, Y. 1993 A theoretical study of polydisperse liquid-sprays in a free shear-layer flow. *Phys. Fluids* A **5**, 3085–3098.

Katoshevski, D. & Tambour, Y. 1995 Sprays in radially spreading shear-layer flows. *Phys. Fluids* **7**, 530–538.

Khosid, S. & Tambour, Y. 1993 New closed-form analytical solutions of the discrete coagulation equation with simultaneous evaporation, and their use for validation of sectional solutions. *Atomization Spray* **3**, 223–248.

Langhaar, H. L. 1942 Steady flow in the transition length of a straight tube. *J. Appl. Mech.* **9**, A55–A58.

Laurent, F. 2006 Numerical analysis of Eulerian multi-fluid models in the context of kinetic formulations for dilute evaporating sprays. *ESAIM – Math. Model. Numer. Anal.* **40**, 431–468.

Laurent, F. & Massot, M. 2001 Multi-fluid modelling of laminar polydisperse spray flame: origin, assumptions and comparison of sectional and sampling methods. *Combust. Theor. Model.* **5**, 537–572.

Laurent, F., Santoro, V., Noskov, M., Smooke, M. D., Gomez, A. & Massot, M. 2004 Accurate treatment of size distribution effects in polydisperse spray diffusion flames: multi-fluid modeling, computations and experiments. *Combust. Theor. Model.* **8**, 385–412.

Leboissetier, A., Okong'o, N. & Bellan, J. 2005 Consistent large-eddy simulation of temporal mixing layer laden with evaporating drops. Part 2. *A posteriori* modelling. *J. Fluid Mech.* **523**, 37–78.

Le Clercq, P. C. & Bellan, J. 2005 Direct numerical simulation of gaseous mixing layers laden with multicomponent-liquid drops: liquid-specific effects. *J. Fluid Mech.* **533**, 57–94.

Liu, J. 1974 Flow of a Bingham fluid in the entrance region of an annular tube. Master's thesis, University of Wisconsin, Milwaukee.

Marble, F. E. 1963 Dynamics of a gas containing small solid particles. *Proc. 5th AGARD Combustion and Propulsion Colloquium (1962),* pp. 175–215.

Matas, J.-P., Glezer, Guazzelli, É. & Morris, J. F. 2004*a* Trains of particles in finite-Reynolds-number pipe flow. *Phys. Fluids* **16**, 4192–4195.

Matas, J.-P., Morris, J. F. & Guazzelli, É. 2004*b* Inertial migration of rigid spherical particles in Poiseuille flow. *J. Fluid Mech.* **515**, 171–195.

Meng, H., Hsiao, G. C., Yang, V. & Shuen, J. S. 2005 Transport and dynamics of liquid oxygen droplets in supercritical hydrogen streams. *J. Fluid Mech.* **527**, 115–139.

Miller, R. S. & Bellan, J. 1999 Direct numerical simulation of a confined three-dimensional gas mixing layer with one evaporating hydrocarbon-droplet-laden stream. *J. Fluid Mech.* **384**, 293–338.

Nakamura, M., Akamatsu, F., Kurose, R. & Katsuki, M. 2005 Combustion mechanism of liquid fuel spray in a gaseous flame. *Phys. Fluids* **17**, 123301.

Nekhamkina, O. A. & Rotinjan, M. A. 1978 Analysis of heat transfer in turbulent flow of multicomponent gases in tubes. *J. Engng Phys.* **33**, 678–686 (in Russian).

Patankar, S. V. & Spalding, D. B. 1967 A finite-difference procedure for solving the equations of the two-dimensional boundary layer. *Intl J. Heat Mass Transfer* **33**, 678–686.

Réveillon, J. & Vervisch, L. 2005 Analysis of weakly turbulent dilute-spray flames and spray combustion regimes. *J. Fluid Mech.* **537**, 317–347.

Saffman, P. G. 1962 On the stability of laminar flow of a dusty gas. *J. Fluid Mech.* **13**, 120–128.

Schonberg, J. A. & Hinch, E. J. 1989 Inertial migration of a sphere in Poiseuille flow. *J. Fluid Mech.* **203**, 517–524.

Segré, G. & Silberberg, A. 1962 Behaviour of macroscopic rigid spheres in Poiseuille flow. *J. Fluid Mech.* **14**, 115–157.

Shah, R. K. & London, A. L. 1978 *Laminar Flow Forced Convection in Ducts*. Academic.

Shumway, R. W. & McEligot, D. M. 1971 Heated laminar gas flow in annuli with temperature-dependent transport properties. *Nucl. Sci. Engng* **46**, 394–399.

Silverman, I., Greenberg, J. B. & Tambour, Y. 1991 Asymptotic analysis of a premixed polydisperse spray flame. *SIAM J. Appl. Maths* **51**, 1284–1303.

Sivashinsky, G. I. 1988 Cascade-renormalization theory of turbulent flame speed. *Combust. Sci. Technol.* **62**, 77–96.

Soo, S. L. 1990 *Multiphase Fluid Dynamics*. Science Press, Beijing, China.

Sparrow, E. M., Lin, S. H. & Lundgren, T. S. 1964 Flow development in the hydrodynamic entrance region of tubes and ducts. *Phys. Fluids* **7**, 338–347.

Tambour, Y. 1984 Vaporization of polydisperse fuel sprays in a laminar boundary layer flow: a sectional approach. *Combust. Flame* **58**, 103–114.

Tambour, Y. 1985 A lagrangian sectional approach for simulating droplet size distribution of vaporizing fuel sprays in a turbulent jet. *Combust. Flame* **60**, 15–28.

Tambour, Y. 1995 Structure of multisize sprays and its effect on spray flame properties. In *Mechanics and Combustion of Droplets and Sprays* (ed. H. H. Chiu & N. Chigier), pp. 210–234. Begell House.

Tambour, Y. & Katoshevski, D. 1994 Similarity analysis of spray diffusion flames in a unidirectional shear-layer flow. In *Twenty-Fifth Int. Symp. on Combustion*, vol. XXV, pp. 381–388.

Tambour, Y. & Katoshevski, D. 1995 Asymptotic analysis of droplet coalescence effects on spray diffusion flames in a unidirectional shear-layer flow. *Atomization Spray* **5**, 357–386.

Tambour, Y. & Zehavi, S. 1993 Derivation of near-field sectional equations for the dynamics of polydisperse spray flows: an analysis of the relaxation zone behind a normal shock wave. *Combust. Flame* **95**, 383–409.

Ulrichson, D. L. & Schmitz, R. A. 1965 Laminar-flow heat transfer in the entrance region of circular tubes. *Intl J. Heat Mass Transfer* **8**, 253–258.

Varanasi, K. K., Clack, H. L. & Miller, R. S. 2004 On preferential diffusion of binary component liquid droplets evaporating in a two-phase mixing layer. *Intl J. Multiphase Flow* **30**, 1235–1257.

Ward-Smith, A. J. 1980 *Internal Fluid Flow: the Fluid Dynamics of Flow in Pipes and Ducts*. Clarendon.

Wolfram, S. 1991 *Mathematica: A System for Doing Mathematics by Computer*. Addison-Wesley.

Yu, K. M., Sung, C. J. & Law, C. K. 1994 Some aspects of the freely propagating premixed flame in a spatially periodic flow field. *Combust. Flame* **97**, 375–383.